Eur. Phys. J. D (2015) 69: 116
DOI: 10.1140/epjd/e2015-50908-y

THE EUROPEAN PHYSICAL JOURNAL D

Regular Article

Comparative analysis of the secondary electron yield from carbon nanoparticles and pure water medium*

Alexey Verkhovtsev[1,2,a], Sally McKinnon[3], Pablo de Vera[4,5], Eugene Surdutovich[6], Susanna Guatelli[3,7], Andrei V. Korol[1,8], Anatoly Rosenfeld[3,7], and Andrey V. Solov'yov[1,2]

[1] MBN Research Center, Altenhöferallee 3, 60438 Frankfurt am Main, Germany
[2] A.F. Ioffe Physical-Technical Institute, Politekhnicheskaya ul. 26, 194021 St. Petersburg, Russia
[3] Centre for Medical Radiation Physics (CMRP), University of Wollongong, NSW, Australia
[4] Departament de Física Aplicada, Universitat d'Alacant, Alicante, Spain
[5] Department of Physical Sciences, The Open University, Milton Keynes, UK
[6] Department of Physics, Oakland University, Rochester, Michigan 48309, USA
[7] Illawarra Health and Medical Research Institute (IHMRI), University of Wollongong, NSW, Australia
[8] Department of Physics, St. Petersburg State Maritime Technical University, Leninskii pr. 101, 198262 St. Petersburg, Russia

Received 23 December 2014 / Received in final form 24 February 2015
Published online 23 April 2015 –

Abstract. The production of secondary electrons generated by carbon nanoparticles and pure water medium irradiated by fast protons is studied by means of model approaches and Monte Carlo simulations. It is demonstrated that due to a prominent collective response to an external field, the nanoparticles embedded in the medium enhance the yield of low-energy electrons. The maximal enhancement is observed for electrons in the energy range where plasmons, which are excited in the nanoparticles, play the dominant role. Electron yield from a solid carbon nanoparticle composed of fullerite, a crystalline form of C_{60} fullerene, is demonstrated to be several times higher than that from liquid water. Decay of plasmon excitations in carbon-based nanosystems thus represents a mechanism of increase of the low-energy electron yield, similar to the case of sensitizing metal nanoparticles. This observation gives a hint for investigation of novel types of sensitizers to be composed of metallic and organic parts.

1 Introduction

Radiotherapy is currently one of the most frequently used technologies to treat tumors, which are a major health concern [1]. However, this technique has a limitation which comes from the sensitivity of healthy tissues, surrounding the tumor, to radiation. To make the treatment more efficient, one needs to minimize the dose delivered to the healthy tissue, thus preventing harmful effects of radiation exposure. Therefore, approaches that enhance radiosensitivity within tumors relative to normal tissues have the potential to become advantageous radiotherapies. A search for such approaches is within the scope of several ongoing multidisciplinary projects [2,3].

One of the most promising modern treatment techniques is ion-beam cancer therapy (IBCT) [4–6]. In this technique, radiation damage is initiated by fast ions incident on tissue. Propagating through the medium, the projectiles deposit their kinetic energy due to the ionization and excitation processes. Biodamage due to ionizing radiation involves a number of phenomena, which happen on various spatial, time, and energy scales. The key phenomena can be described within the so-called multiscale approach to the physics of radiation damage with ions (see Ref. [7] and references therein). As a result of the interaction of projectiles with the medium, secondary particles, such as electrons, free radicals, etc., are produced. By now, it is generally accepted that the vast portion of biodamage done by incident heavy ions is related to these secondary particles [7–10]. Particularly, the low-energy electrons, having the kinetic energy from a few eV to several tens of eV, have been shown to act as important agents of biodamage [11,12].

Metallic nanoparticles, especially those composed of noble metals, were proposed recently to act as sensitizers in cancer treatments with ionizing radiation [13–17]. Such nanoagents delivered to the tumor region can boost the production of secondary electrons near the target [18,19]. The enhanced production of low-energy electrons will also lead to an increase in the number of free radicals [20] as well as other reactive species, like hydrogen peroxide H_2O_2 [21], which can propagate from the cytoplasm to the cell nucleus. Thus, these species can deliver damaging impacts onto the DNA from the radiation induced damages associated with the presence of nanoparticles in other

* Contribution to the Topical Issue "COST Action Nano-IBCT: Nano-scale Processes Behind Ion-Beam Cancer Therapy", edited by Andrey V. Solov'yov, Nigel Mason, Gustavo Garcia and Eugene Surdutovich.

[a] e-mail: verkhovtsev@fias.uni-frankfurt.de

cell compartments [22]. An enhanced production of the secondary species will lead to an increase of the relative biological effectiveness of ionizing radiation. This quantity is defined as the ratio of the dose delivered by photons to that delivered by different radiation modalities, leading to the same biological effects, such as the probability of an irradiated cell inactivation.

The physical mechanisms of enhancement of the electron yield from sensitizing nanoparticles are still a debated issue. In the recent studies [23,24], it was discovered that a significant increase in the number of emitted electrons due to irradiation of noble metal nanoparticles by fast ions comes from the two distinct types of collective electron excitations. It was demonstrated that the yield of the 1–10 eV electrons is strongly enhanced due to the decay of plasmons, i.e. collective excitations of delocalized valence electrons in metallic nanoparticles. For electron energies of about 10–30 eV, the dominating contribution to the electron yield arises from the atomic giant resonance associated with the excitation of d-electrons in individual atoms in a nanoparticle [23].

Excitation of plasmons by time-dependent external electric fields is a characteristic feature of not only metallic but also, to some extent, of carbon nanoscale systems. For instance, it is generally accepted that plasmon excitations dominate the spectra of photo- and electron impact ionization of fullerenes [25–30] and polycyclic aromatic hydrocarbons (PAHs) [31,32].

In this paper, we demonstrate that the decay of plasmons excited in carbon nanoparticles also plays a prominent role in the production of low-energy electrons. Due to the collective response to a time-dependent external electric field, these systems enhance the production of secondary electrons in a biological medium, in the energy range where the plasmons play the dominant role. This is done by the calculation of spectra of secondary electrons ejected from a carbon nanoparticle composed of fullerite, a crystalline form of C_{60} fullerene, irradiated by fast protons. The contribution of plasmon excitations to the electron production is evaluated by means of the plasmon resonance approximation [33–36]. The results of these calculations are compared to the model calculations based on the dielectric formalism [37] and Monte Carlo simulations [38,39], carried out for pure water medium and for the medium with an embedded carbon nanoparticle. Utilizing and comparing different theoretical and numerical methods, we provide a recipe for evaluation of the electron production in the kinetic energy range from a few eV to thousands of eV. A single method does not allow one to properly quantify the secondary electron yield in a broad energy range; thus, a combination of different approaches is required.

2 Theory and computational details

2.1 Plasmon resonance approximation

The contribution of collective electron excitations to the ionization spectra of carbon nanoparticles is evaluated by means of the plasmon resonance approximation (PRA) (see Refs. [33–36] and references therein). This approach postulates that the dominating contribution to the ionization cross section in the vicinity of the plasmon resonance comes from collective electron excitations, while single-particle effects give a small contribution compared to the collective modes [40,41]. In the past, this approach has provided a clear physical explanation of the resonant-like structures in photoionization spectra [30,34] and differential inelastic scattering cross sections [27,28,42,43] of metallic clusters and carbon fullerenes irradiated by photons and fast electrons.

To start with, we evaluate the plasmon contribution to the ionization spectrum of an isolated C_{60} molecule. Within the utilized model, the fullerene is represented as a spherical "jellium" shell of a finite width, $\Delta R = R_2 - R_1$, so the electron density is homogeneously distributed over the shell with thickness ΔR [26,44,45]. The chosen value, $\Delta R = 1.5$ Å, corresponds to the size of the carbon atom [44].

The interaction of a hollow system with a non-uniform electric field, created in collisions with charged projectiles, leads to the time-dependent variation of the electron density appearing on the inner and outer surfaces of the hull as well as in its interior [36]. This variation leads to the formation of a surface plasmon, which has two normal modes, the symmetric and antisymmetric [26,44–46], and of a volume plasmon [41], which occurs due to a local compression of the electron density inside the shell. The detailed explanation of formation of different plasmon modes can be found in references [34,36].

The utilized approach relies on several parameters, which include the oscillator strength of the plasmon excitation, position of the plasmon resonance peak, and its width. The choice of these parameters can be justified by comparing the model-based spectra with either experimental data or the results of more advanced ab initio calculations. As a benchmark of the utilized approach, the photo- and electron impact ionization cross sections of carbon-based systems, namely fullerenes and PAHs, were calculated recently [28,30,32,43]. The results obtained for C_{60} [28,30,43] agreed well with experimental data on photoionization [29] and electron inelastic scattering [28,43]. Being a clear physical model which describes collective electron excitations, the PRA has been proven to be a useful tool for interpretation of experimental results and making new numerical estimates.

Within the PRA, the double differential inelastic scattering cross section of a fast projectile in collision with a hull-like system can be defined as a sum of three terms [28,36] (hereafter, we use the atomic system of units, $m_e = |e| = \hbar = 1$):

$$\frac{d^2\sigma_{\rm pl}}{d\varepsilon_2 d\Omega_{\mathbf{p}_2}} = \frac{d^2\sigma^{(s)}}{d\varepsilon_2 d\Omega_{\mathbf{p}_2}} + \frac{d^2\sigma^{(a)}}{d\varepsilon_2 d\Omega_{\mathbf{p}_2}} + \frac{d^2\sigma^{(v)}}{d\varepsilon_2 d\Omega_{\mathbf{p}_2}}, \quad (1)$$

which describe the partial contribution of the surface (the two modes, s and a) and the volume (v) plasmons. Here ε_2 is the kinetic energy of the scattered projectile, $\mathbf{p}_2$ its momentum, and $\Omega_{\mathbf{p}_2}$ its solid angle. The cross section $d^2\sigma_{\rm pl}/d\varepsilon_2 d\Omega_{\mathbf{p}_2}$ can be written in terms of the energy loss

$\Delta\varepsilon = \varepsilon_1 - \varepsilon_2$, of the incident particle of energy ε_1. Integration of $d^2\sigma_{\rm pl}/d\Delta\varepsilon\, d\Omega_{\mathbf{p}_2}$ over the solid angle leads to the single differential cross section:

$$\frac{d\sigma_{\rm pl}}{d\Delta\varepsilon} = \int d\Omega_{\mathbf{p}_2} \frac{d^2\sigma_{\rm pl}}{d\Delta\varepsilon\, d\Omega_{\mathbf{p}_2}} = \frac{2\pi}{p_1 p_2} \int_{q_{\rm min}}^{q_{\rm max}} q\, dq \frac{d^2\sigma_{\rm pl}}{d\Delta\varepsilon\, d\Omega_{\mathbf{p}_2}}, \tag{2}$$

where $\mathbf{p}_1$ is the initial momentum of the projectile and $\mathbf{q} = \mathbf{p}_1 - \mathbf{p}_2$ is the transferred momentum. Explicit expressions for the contributions of the surface and volume plasmons, entering equation (1), obtained within the plane-wave Born approximation, are presented in reference [36]. The Born approximation is applicable since the considered collision velocities (v_1 = 2–20 a.u.) substantially exceed the characteristic velocities of delocalized electrons in the fullerene ($v_e \approx 0.7$ a.u.).

The surface and volume plasmon terms appearing on the right-hand side of equation (1) are constructed as a sum over different multipole contributions corresponding to different values of the angular momentum l:

$$\frac{d^2\sigma^{(i)}}{d\varepsilon_2 d\Omega_{\mathbf{p}_2}} \propto \sum_l \frac{\omega_l^{(i)2}\, \Gamma_l^{(i)}}{\left(\omega^2 - \omega_l^{(i)2}\right)^2 + \omega^2 \Gamma_l^{(i)2}},$$
$$\frac{d^2\sigma^{(v)}}{d\varepsilon_2 d\Omega_{\mathbf{p}_2}} \propto \sum_l \frac{\omega_p^2\, \Gamma_l^{(v)}}{\left(\omega^2 - \omega_p^2\right)^2 + \omega^2 \Gamma_l^{(v)2}}, \tag{3}$$

where $i = s, a$ denotes the two modes of the surface plasmon. Their frequencies are given by [36,44]:

$$\omega_l^{(s/a)} = \left(1 \mp \frac{1}{2l+1}\sqrt{1 + 4l(l+1)\xi^{2l+1}}\right)^{1/2} \frac{\omega_p}{\sqrt{2}}, \tag{4}$$

where '−' and '+' stand for symmetric (s) and antisymmetric (a) modes, respectively, and $\xi = R_1/R_2$ is the ratio of the inner to the outer radii of the shell. The volume plasmon frequency ω_p, associated with the ground-state electron density ρ_0, is given by

$$\omega_p = \sqrt{4\pi\rho_0} = \sqrt{\frac{3N}{R_2^3(1-\xi^3)}}, \tag{5}$$

where N is the number of delocalized electrons involved in the collective excitation. In the case of a fullerene C_n, the number N of delocalized electrons represents the four $2s^2 2p^2$ valence electrons from each carbon atom. Thus, we assume that 240 delocalized electrons of C_{60} contribute to the formation of plasmons.

In reference [42] it was shown that the excitations with large angular momenta have a single-particle rather than a collective nature. With increasing l, the wavelength of plasmon excitation, $\lambda_{\rm pl} = 2\pi R/l$, becomes smaller than the characteristic wavelength of the delocalized electrons in the system, $\lambda_e = 2\pi/\sqrt{2\epsilon}$. Here ϵ is the characteristic electron excitation energy in the cluster, $\epsilon \sim I_p$, and I_p is the ionization threshold of the system ($I_p(C_{60}) \sim 7.5$ eV [25]). In the case of the C_{60} fullerene, the estimates show that the excitations with $l > 3$ are formed by single electron transitions rather than by the collective ones. Therefore, only terms corresponding to the dipole ($l = 1$), quadrupole ($l = 2$) and octupole ($l = 3$) plasmon terms have been accounted for in the sum over l in equation (3).

Table 1. Peak positions of the surface and the volume plasmon modes as well as their widths used in the present calculations. All values are given in eV.

	$l=1$	$l=2$	$l=3$
$\omega_l^{(s)}$	19.0	25.5	30.5
$\Gamma_l^{(s)}$	11.4	15.3	18.3
$\omega_l^{(a)}$	33.2	31.0	29.5
$\Gamma_l^{(a)}$	33.2	31.0	29.5
ω_p		37.1	
$\Gamma_l^{(v)}$		37.1	

Following the methodology utilized in reference [43], we assume that the ratio $\gamma_l = \Gamma_l/\omega_l$ of the width of the plasmon resonance to its frequency equals to $\gamma_l^{(s)} = 0.6$ for all multipole terms of the symmetric mode, and to $\gamma_l^{(a)} = 1.0$ for the antisymmetric mode. These values were utilized previously to describe experimental data on photoionization [29] and electron inelastic scattering [28,43] of gas-phase C_{60}. The value $\gamma_l^{(s)} = 0.6$ is also close to the numbers obtained from the earlier photoionization and electron energy loss experiments on neutral C_{60} [25,27]. The value $\gamma_l^{(a)} = 1.0$ is consistent with the widths of the second plasmon resonance observed in the photoionization of C_{60}^{q+} (q = 1–3) ions [47]. For the volume plasmon, we consider the ratio $\gamma_l^{(v)} = \Gamma_l^{(v)}/\omega_p = 1.0$. The values of the plasmon resonance peaks and the widths are summarized in Table 1.

2.2 Dielectric formalism

The secondary electron production in a pure water medium as well as in a carbon nanoparticle was investigated by means of a model approach based on the dielectric formalism [37]. This method relies on experimental measurements of the energy-loss function of the target medium, $\mathrm{Im}[-1/\epsilon(\omega, q)]$, where $\epsilon(\omega, q)$ is the complex dielectric function, with ω and q being the energy and the momentum transferred to the electronic excitation, respectively. In reference [48], this approach was used to obtain spectra of secondary electrons generated in liquid water by energetic ions. An alternative method to calculate the impact ionization cross sections of various biological media was proposed recently [49,50]. Instead of calculating the exact energy-loss function and ionization threshold for different electronic shells of a molecule composing the target medium, this approach aims at calculating the mean value of the binding energies for several outer shells. It is assumed that ionization of these shells happens if the energy transferred to the medium exceeds this mean value

of the binding energies [49]. The formalism presented allows one to calculate the cross sections not only for liquid water but also for a real biological medium containing sugars, amino acids, etc. In particular, it was utilized recently [51] to study ionization and energy deposition in different subcellular compartments, such as cell nucleus and cytoplasm, due to proton irradiation. In this work, we apply this formalism to study the electron production from a nanoparticle composed of fullerite.

2.3 Monte Carlo simulation of secondary electron yield

Monte Carlo simulations of secondary electron production in a nanoparticle were performed using Geant4, version 9.6 patch 1 [38,39]. The simulation geometry consisted of a 50 nm diameter spherical nanoparticle of variable material placed at the center of a 5 μm world of liquid water. A 4 μm sided cube was included to allow the use of different secondary particle production thresholds in different regions in order to optimize execution times. Monoenergetic protons propagating from a point source were incident from the edge of the nanoparticle.

The material of the nanoparticle was simulated as liquid water or a customized fullerene material alternatively. The fullerene material properties were set by scaling the density of the Geant4 element carbon according to the calculated density of a face-centered cubic (*fcc*) structure of fullerite.

The Low Energy Electromagnetic Physics Package [52], using the Livermore Data Libraries, was selected to model the interactions of electrons and photons in the nanoparticle. Models describing proton interactions in the nanoparticle were selected following the Geant4 advanced example "Microdosimetry". The ionization model implemented for protons was the Geant4 "BraggIonGas" model, valid for protons kinetic energy up to 2 MeV, while the Bethe-Bloch model was adopted for higher energies. In the nanoparticle, nuclear stopping power was modeled using the Geant4 "ICRU49NucStopping" model. The multiple scattering was modeled for all charged particles with the Geant4 "UrbanMsc95" model [52]. Atomic de-excitation (fluorescence and Auger electrons) was modeled as well [53]. Secondary electron production from the nanoparticle is limited to the electrons with kinetic energy greater than 250 eV as this is the low-energy limit of validity of the Livermore Data Libraries [54].

The Geant4-DNA Very Low Energy extensions [55] were adopted in liquid water surrounding the nanoparticle to model in detail particle interactions down to a few eV scale. Physical interactions modeled for protons in the water sphere were G4DNAExcitation, G4DNAIonisation, and G4DNAChargeDecrease. The models used are the default Geant4-DNA model classes.

The simulations in this study modeled the interactions of 1 MeV protons generated from one position and in one direction incident on the nanoparticle. Secondary electrons were produced in the nanoparticle with a cut of 250 eV. The cut is the threshold of production of secondary particles. Below the cut, secondary electrons are not produced and their energy is deposited locally, while above the cut, secondary electrons are produced and tracked in the nanoparticle and in the surrounding medium. The kinetic energy spectra of secondary electrons escaping the nanoparticle were retrieved and the spectra at creation was compared directly to the same physical quantity calculated by means of the analytical model. The proportion of escaping secondary electrons produced within the fullerite-like nanoparticle was 98.5%.

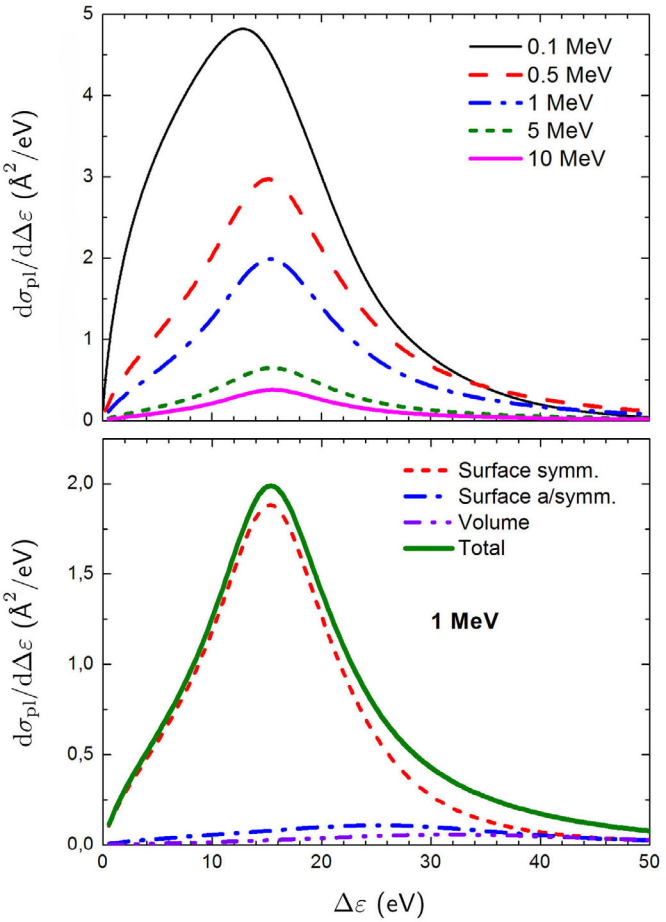

Fig. 1. Upper panel: contribution $d\sigma_{pl}/d\Delta\varepsilon$ of the plasmon excitations to the single differential cross section of C_{60} fullerene irradiated by fast protons of different incident energies as a function of the energy loss. Lower panel illustrates the contribution of different plasmon excitations to the cross section $d\sigma_{pl}/d\Delta\varepsilon$ of C_{60} irradiated by a 1 MeV proton.

3 Results and discussion

3.1 Electron production by an isolated C_{60} molecule due to the plasmon excitation mechanism

The upper panel of Figure 1 illustrates the single differential cross section $d\sigma_{pl}/d\Delta\varepsilon$ calculated by means of the PRA for the C_{60} fullerene irradiated by fast protons of different incident energies as indicated. The presented

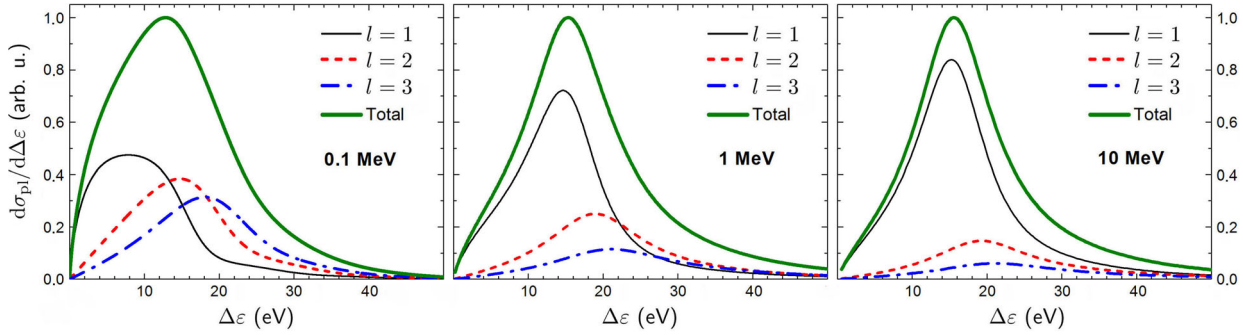

Fig. 2. Relative contribution of different multipole terms to the single differential cross section $d\sigma_{pl}/d\Delta\varepsilon$ of C_{60} fullerene irradiated by 0.1, 1, 10 MeV protons as a function of the energy loss.

spectra comprise contributions of both the surface and volume plasmon excitations of different angular momenta l. As mentioned in Section 2.1, we have accounted for the dipole ($l = 1$), quadrupole ($l = 2$), and octupole ($l = 3$) plasmon terms because the excitations with higher angular momentum are formed by single electron transitions rather than by the collective ones. The contribution of different plasmon modes to the spectrum of C_{60} irradiated by a 1 MeV proton is illustrated in the lower panel of Figure 1. The main contribution to the cross section comes from the symmetric mode of the surface plasmon, whose relative contribution exceeds that of the volume plasmon by about an order of magnitude. The similar trend was observed recently studying electron production by noble metal nanoparticles [23,24]. Thus, the leading mechanism of electron production by sensitizing nanoparticles due to the plasmon excitations should be related to the surface term but not to the volume one.

Figure 1 demonstrates that the amplitude and the shape of the plasmon resonance depend strongly on the kinetic energy of protons. It was shown previously [42] that the relative contributions of the quadrupole and higher multipole terms to the cross section decrease significantly with an increase of the collision velocity. At high velocities, the dipole term dominates over the contributions of larger l, since the dipole potential decreases slower at large distances than the higher multipole potentials. To illustrate this effect, we have plotted the partial contributions of different multipole modes which are excited due to irradiation by 0.1, 1, and 10 MeV protons. These dependencies are presented in Figure 2. For the sake of clarity, the cross sections, which represent the sum of three multipole contributions, have been normalized to unity at the point of maximum. Thus, one can compare directly the relative contribution of the different terms to the cross section at different incident energies. A prominent interplay of the different multipole terms at the lowest incident energy (left panel) results in a shift in the position of the maximum of the cross section.

To quantify the production of electrons in collision with a nanoparticle, we redefine the cross section $d\sigma/d\Delta\varepsilon$ as a function of the kinetic energy W of emitted electrons. This quantity is related to the energy loss via $W = \Delta\varepsilon - I_p$, where I_p is the ionization threshold of the system. The first ionization potential of the C_{60} fullerene approximately equals to 7.5 eV [25].

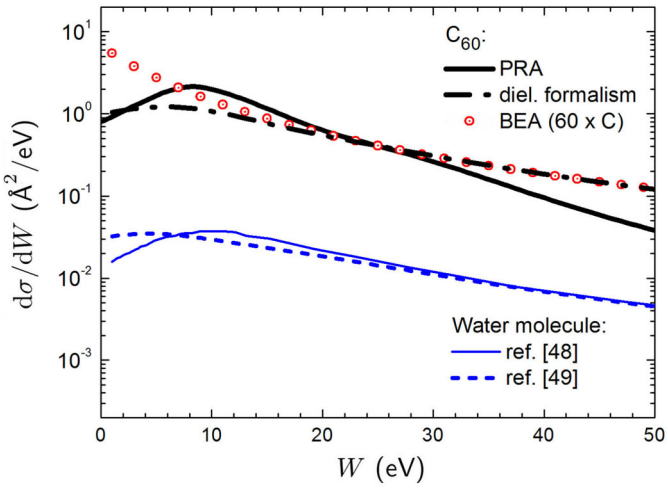

Fig. 3. Single differential cross section $d\sigma/dW$ of the C_{60} fullerene (thick solid and dash-dotted black curves) and of a water molecule (thin solid and dashed blue curves) irradiated by a 1 MeV proton as a function of the kinetic energy of emitted electrons. Thick solid (black) curve illustrates the contribution of the plasmon excitations to the emission spectrum from C_{60}. Thin solid and dashed (blue) curves represent the results obtained within the dielectric formalism by Scifoni et al. [48] and de Vera et al. [49], respectively. Symbols represent the cross section of a single C atom calculated by means of BEA, multiplied by 60.

Figure 3 shows the cross section $d\sigma/dW$ of C_{60} (thick solid and dash-dotted black curves) and of a water molecule (thin solid and dashed blue curves) irradiated by a 1 MeV proton as a function of the kinetic energy of emitted electrons. The results for water obtained within the dielectric formalism are taken from references [48,49]. The thick solid curve demonstrates the contribution of the plasmon excitations to the spectrum of C_{60}, $d\sigma_{pl}/dW$, calculated within the PRA approach. The dash-dotted curve represents the results obtained within the dielectric formalism. In the latter case, we took the experimental optical energy-loss function of fullerite [56] and calculated the mean binding energy of the outer-shell electrons.

The binding energies of the valence orbitals of C_{60} were taken from the ab initio calculations of Deutsch et al. [57]. Symbols show the cross section $d\sigma/dW$ for the 1 MeV proton impact of a single carbon atom calculated by means of the binary encounter approximation (BEA) [58,59], multiplied by 60. The results of the calculations based on the dielectric formalism agree well with those within the BEA at the energy of about 20 eV and above. This indicates that the emission of electrons with kinetic energy of about several tens of eV takes place via single-electron excitations of the system. The plasmon excitations dominate the spectrum at lower energies, i.e. in the vicinity of the plasmon resonance, while this contribution drops off at higher energies of emitted electrons. In the energy range where the plasmons are excited, single-particle effects give a small contribution as compared to the collective modes. At higher energies, the collective excitation decays to the incoherent sum of single-electron excitations. Note that at lower electron energies (from 1 to approximately 20 eV) the BEA-based results start to deviate significantly from that of the dielectric formalism. This deviation indicates that the BEA is not applicable for the description of low-energy electron emission, since these electrons are produced in distant rather than in binary collisions. In this energy range, the PRA approach better describes the low-energy electron emission since it accounts for the collective electron effects omitted in other models.

3.2 Electron production by a large carbon nanoparticle

In the previous section, we have calculated the single differential cross section for an isolated C_{60} molecule within the PRA approach and the dielectric formalism. Now, we we apply these methods as well as the Monte Carlo scheme to study the production of secondary electrons by a large solid carbon nanoparticle whose density corresponds to that of fullerite, the crystalline form of C_{60}.

The single differential cross section $d\sigma/dW$ can be related to the probability to produce N secondary electrons with kinetic energy W, in the interval dW, emitted from a segment Δx of the trajectory of a single ion [7,60]:

$$\frac{dN(W)}{dW} = n\Delta x \frac{d\sigma}{dW}, \tag{6}$$

where n is the atomic density of a system of compounds,

$$n = \frac{\rho}{N_{\rm at}\, m_{\rm at}}, \tag{7}$$

with ρ being the mass density of a target, $N_{\rm at}$ the number of atoms in the target compound, and $m_{\rm at}$ the atomic mass.

As a case study, we have considered a nanoparticle of 50 nm in diameter. In the calculations, we assumed that (i) C_{60} molecules in fullerite are packed in the fcc crystalline lattice, and (ii) a unit cell is composed of four C_{60} molecules. Knowing the lattice parameter of fullerite, $a = 1.417$ nm, and the mass of a single carbon atom, $m_{\rm C} = 12$ u, we have calculated the density of the fullerite crystal:

$$\rho(\text{fullerite}) = \frac{4 \times 60 m_{\rm C}}{a^3} = 1.68 \text{ g/cm}^3. \tag{8}$$

Utilizing these values, we have obtained the atomic density of fullerite:

$$n(\text{fullerite}) = \frac{\rho(\text{fullerite})}{60 m_{\rm C}} = 1.4 \times 10^{21} \text{ cm}^{-3}, \tag{9}$$

which is by about an order of magnitude smaller than that of water, $n(\text{water}) = 3.34 \times 10^{22}$ cm^{-3}.

In Figure 4, we compare the electron yield from a 50 nm spherical carbon nanoparticle and from the equivalent volume of pure water medium. We have calculated the number of electrons per unit energy produced due to

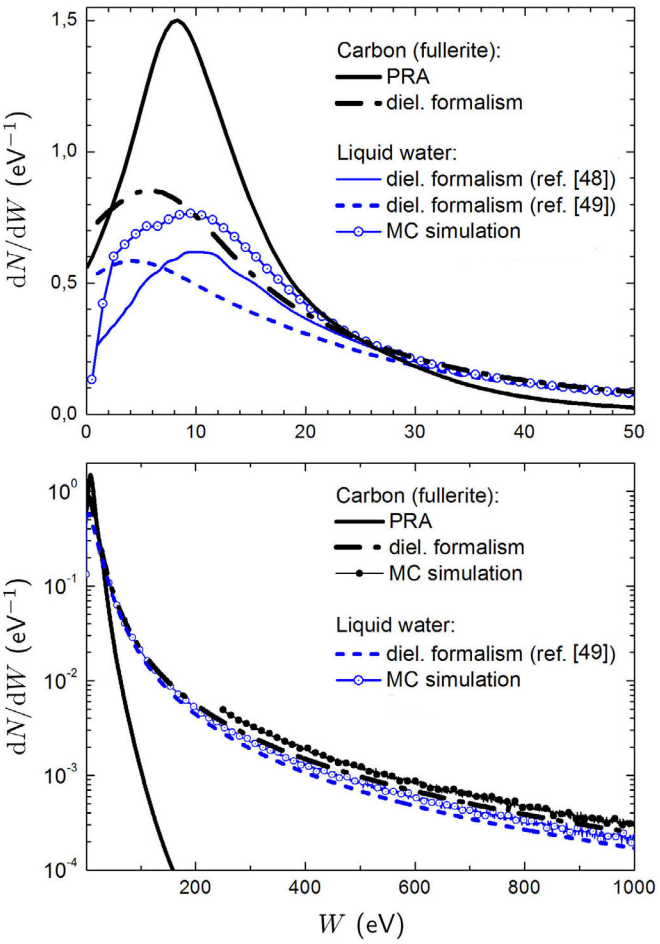

Fig. 4. Number of electrons per unit energy produced by irradiation of a 50 nm carbon nanoparticle by a single 1 MeV proton (black curves and filled circles). Blue curves represent the number of electron generated in the equivalent volume of liquid water. Solid and dashed blue curves represent the results obtained within the dielectric formalism by Scifoni et al. [48] and de Vera et al. [49], respectively. Open circles illustrate this quantity obtained on the basis of Monte Carlo simulations using the Geant4-DNA simulation tool.

irradiation by a 1 MeV proton. Thick black curve represents the contribution of collective electron excitations estimated by means of the PRA. The dash-dotted black curve shows the number of electrons estimated by means of the dielectric formalism. Filled and open symbols represent the results of the Monte Carlo simulations carried out by means of the Geant4 tool for the carbon nanoparticle and pure water medium, respectively. Thin solid and dashed blue curves represent the results of recent calculation for liquid water obtained within the dielectric formalism [48,49]. Note that in the Monte Carlo simulations, we did not simulate the crystalline lattice of fullerite explicitly but the material properties were set by scaling the density of the Geant4 element carbon according to the calculated density ρ (fullerite).

Comparative analysis of the spectra at low kinetic energy of emitted electrons (the upper panel of Fig. 4) demonstrates that the number of electrons with the energy of about 10 eV, produced by the carbon nanoparticle *via the plasmon excitation mechanism*, is several times higher than that created in pure water. The enhancement of the yield of low-energy electrons may increase the probability of the tumor cell killing due to the double- or multiple strand break of the DNA [7]. Similar to the case of noble metal nanoparticles [13–17], the use of carbon-based nanostructures in cancer treatments with ionizing radiation can thus produce the sensitization effect. As it was shown recently [23,24], the number of electrons with the energy of about a few eV produced by the noble metal (gold and platinum) nanoparticles via the plasmon excitation mechanism exceeds that generated in the same volume of liquid water by an order of magnitude. In the case of a carbon nanoparticle, the electron yield reaches the maximum at higher electron energies, namely at about 10 eV. Assuming this, one can consider novel metal-organic sensitizing nanoparticles, where collective excitations will arise in both parts of the system. A proper choice of the constituents will allow one to tune the position of the resonance peaks in the ionization spectra of such systems and, subsequently, to cover a broader kinetic energy spectrum of electrons emitted from such nanoparticles. The fabrication of new, more efficient types of sensitizers would allow one to significantly advance modern techniques of cancer treatment with ionizing radiation.

In the case of electrons with higher kinetic energy (the lower panel of Fig. 4), the effect done by the carbon nanoparticle (filled symbols and dash-dotted black curve) is also more prominent as compared to pure water (open symbols and dashed blue curve), as follows from both the calculations based on the dielectric formalism and the Monte Carlo simulations. As discussed above, the contribution of the plasmon excitations rapidly decreases at the energies exceeding approximately 30 eV. The PRA accounts only for collective electron excitations that dominate the ionization spectra at low energies. At higher energies, the plasmons decay into the incoherent sum of single-electron excitations whose contribution is the most prominent in this energy region.

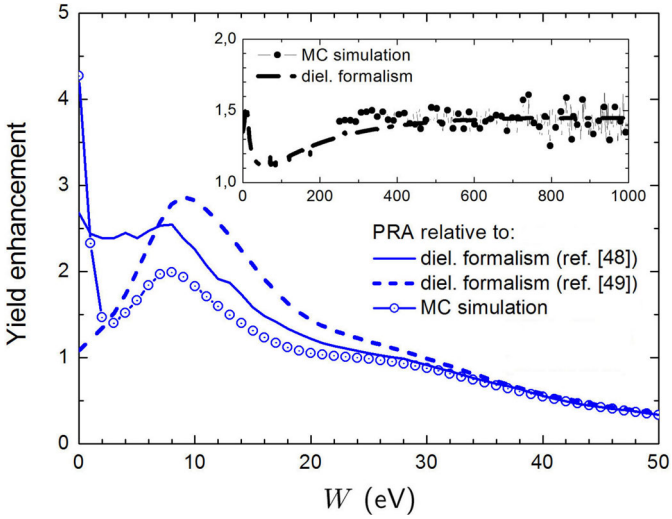

Fig. 5. Yield enhancement from the 50 nm carbon nanoparticle as compared to pure water medium. Solid and dashed blue lines show the enhancement due to the plasmon excitations as compared to the results obtained within the dielectric formalism by Scifoni et al. [48] and de Vera et al. [49], respectively. Open symbols illustrate the plasmon-based enhancement compared to the results of Monte Carlo simulations. The enhancement estimated solely by means of the dielectric formalism and the Monte Carlo simulations in a broader kinetic energy range is shown in the inset by the dash-dotted curve and filled symbols, respectively.

In order to quantify the difference in electron production by the carbon nanoparticle and by an equivalent volume of pure water, we have calculated the relative enhancement of the electron yield from the nanoparticle as compared to water. This quantity is presented in Figure 5. The main figure shows the enhancement which was calculated by comparing the contribution of the plasmon excitations, obtained within the PRA, to the electron yield from pure water calculated by means of the dielectric formalism (solid and dashed blue curves) and Monte Carlo simulations (open symbols). Depending on the data to be chosen as a reference, the collective electron excitations result in 2 to 3 times greater number of emitted 10 eV electrons as compared to the case of water. This effect is less pronounced than the enhancement done by small noble metal nanoparticles which can produce up to 15–20 times greater number of electrons via the plasmon decay mechanism as compared to water [23,24]. On the other hand, this enhancement results in an excessive emission of the very low-energy electrons of about a few eV, while the carbon-based nanoparticle can enhance the yield of more energetic electrons. For the sake of completeness, we also demonstrate the enhancement done by the carbon nanoparticle in a broader kinetic energy range (see the inset of Fig. 5). For that purpose, we have compared the electron yields from the two systems calculated by means of the dielectric formalism (dash-dotted curve) and also from the Monte Carlo simulation (filled symbols). The two approaches lead to a similar result, namely that the carbon nanoparticle

enhances the number of energetic (of about hundreds of eV up to 1 keV) secondary electrons by about 50%.

The analysis performed demonstrates that a single theoretical or numerical approach does not allow one to properly quantify the secondary electron yield in a broad kinetic energy range, from a few eV up to a few keV. Thus, one needs to utilize a combination of different methods to achieve this goal. The calculated spectra of secondary electrons can further be used as the input data for investigation of radiobiological effects by means of the multiscale approach to the physics of radiation damage with ions [7]. This approach has the goal of developing knowledge about biodamage at the nanoscale and molecular level and finding the relation between the characteristics of incident particles and the resultant biological damage.

4 Conclusion

We have analyzed numerically the production of electrons by carbon nanoparticles irradiated by fast protons. The study has been carried out by means of the model approaches based on the plasmon resonance approximation and the dielectric formalism, as well as by means of Monte Carlo simulations. It has been demonstrated that due to the prominent collective response to a time-dependent external electric field, carbon-based nanoparticles enhance the production of low-energy electrons via the plasmon excitation mechanism.

The contribution of plasmons to the electron production from a carbon nanoparticle has been compared to the results of model calculations, based on the dielectric formalism, as well as to the results of Monte Carlo simulations for pure water medium. It has been shown that the number of the low-energy electrons (with the kinetic energy of about 10 eV) produced by a 50 nm carbon nanoparticle is several times higher than that emitted from pure water. Similar to the case of sensitizing metallic nanoparticles, the decay of the plasmon excitations formed in carbon nanostructures represents an important mechanism of generation of low-energy electrons. This observation gives an opportunity to fabricate new types of sensitizers, composed of the metallic and the organic parts, where the plasmon excitations will arise in both parts of the system. As a result, it will become possible to cover a broader kinetic energy range of electrons emitted from such systems, as compared to currently proposed nanoagents, and, subsequently, to improve modern techniques of cancer treatment with ionizing radiation.

The work was supported by the COST Action MP1002 “Nanoscale insights into Ion Beam Cancer Therapy” (Nano-IBCT) and by the FP7 Multi-ITN Project “Advanced Radiotherapy, Generated by Exploiting Nanoprocesses and Technologies” (ARGENT) (Grant Agreement No. 608163).

A.V. and P.d.V. performed the calculations within the PRA and the dielectric formalism, respectively, under the supervision of A.V.S. The MC simulations were carried out by S.M. under the supervision of S.G., A.R. and A.V.S. The manuscript was drafted by A.V. and S.M. The PRA-based results were analyzed by A.V., A.V.K. and A.V.S. The results of MC simulations were analyzed by S.M., S.G. and A.R. E.S. actively participated in the discussion of the results and provided valuable comments. All authors contributed extensively to discussions about this work and in reviewing the manuscript.

References

1. G. Delaney, S. Jacob, C. Featherstone, M. Barton, Cancer **104**, 1129 (2005)
2. European COST Action “Nanoscale insights into Ion-Beam Cancer Therapy” (Nano-IBCT), http://www.cost.eu/domains_actions/mpns/Actions/nano-ibct/
3. FP7 Initial Training Network Project “Advanced Radiotherapy, Generated by Exploiting Nanoprocesses and Technologies” (ARGENT), http://www.itn-argent.eu
4. I. Bacarelli, F.A. Gianturco, E. Scifoni, A.V. Solov’yov, E. Surdutovich, Eur. Phys. J. D **60**, 1 (2010)
5. D. Schardt, T. Elsässer, D. Schulz-Ertner, Rev. Mod. Phys. **82**, 383 (2010)
6. M. Durante, J.S. Loeffler, Nat. Rev. Clin. Oncol. **7**, 37 (2010)
7. E. Surdutovich, A.V. Solov’yov, Eur. Phys. J. D **68**, 353 (2014)
8. A.V. Solov’yov, E. Surdutovich, E. Scifoni, I. Mishustin, W. Greiner, Phys. Rev. E **79**, 011909 (2009)
9. B.D. Michael, P. O’Neill, Science **287**, 1603 (2000)
10. S. Denifl, T.D. Märk, P. Scheier, in *Radiation Damage in Biomolecular Systems*, edited by G. Garcia Gomez-Tejedor, M.C. Fuss (Springer Science, Business Media B.V., 2012), p. 45
11. B. Boudaïffa, P. Cloutier, D. Hunting, M.A. Huels, L. Sanche, Science **287**, 1658 (2000)
12. M.A. Huels, B. Boudaïffa, P. Cloutier, D. Hunting, L. Sanche, J. Am. Chem. Soc. **125**, 4467 (2003)
13. D.M. Herold, I.J. Das, C.C. Stobbe, R.V. Iyer, J.D. Chapman, Int. J. Radiat. Biol. **76**, 1357 (2000)
14. J.J. Hainfeld, D.N. Slatkin, H.M. Smilowitz, Phys. Med. Biol. **49**, N309 (2004)
15. S.J. McMahon et al., Sci. Rep. **1**, 18 (2011); (Corrigendum: Sci. Rep. **3**, 1725 (2013))
16. W. Chen, J. Zhang, J. Nanosci. Nanotechnol. **6**, 1159 (2006)
17. E. Porcel, S. Liehn, H. Remita, N. Usami, K. Kobayashi, Y. Furusawa, C. Le Sech, S. Lacombe, Nanotechnology **21**, 085103 (2010)
18. F. Xiao, Y. Zheng, P. Cloutier, Y. He, D. Hunting, L. Sanche, Nanotechnology **22**, 465101 (2011)
19. Y. Zheng, D.J. Hunting, P. Ayotte, L. Sanche, Radiat. Res. **169**, 19 (2008); (Erratum: Radiat. Res. **169**, 481 (2008))
20. C. Sicard-Roselli et al., Small **10**, 3338 (2014)
21. E. Porcel et al., Nanomed. Nanotech. Biol. Med. **10**, 1601 (2014)
22. L. Štefančíková et al., Cancer Nanotech. **5**, 6 (2014)
23. A.V. Verkhovtsev, A.V. Korol, A.V. Solov’yov, Phys. Rev. Lett. **114**, 063401 (2015)
24. A.V. Verkhovtsev, A.V. Korol, A.V. Solov’yov, J. Phys. Chem. C (in print), DOI: 10.1021/jp511419n
25. I.V. Hertel, H. Steger, J. de Vries, B. Weisser, C. Menzel, B. Kamke, W. Kamke, Phys. Rev. Lett. **68**, 784 (1992)
26. Ph. Lambin, A.A. Lucas, J.-P. Vigneron, Phys. Rev. B **46**, 1794 (1992)

27. L.G. Gerchikov, P.V. Efimov, V.M. Mikoushkin, A.V. Solov'yov, Phys. Rev. Lett. **81**, 2707 (1998)
28. A.V. Verkhovtsev, A.V. Korol, A.V. Solov'yov, P. Bolognesi, A. Ruocco, L. Avaldi, J. Phys. B **45**, 141002 (2012)
29. B.P. Kafle, H. Katayanagi, M. Prodhan, H. Yagi, C. Huang, K. Mitsuke, J. Phys. Soc. Jpn **77**, 014302 (2008)
30. A.V. Verkhovtsev, A.V. Korol, A.V. Solov'yov, Phys. Rev. A **88**, 043201 (2013)
31. Y. Ling, C. Lifshitz, Chem. Phys. Lett. **257**, 587 (1996)
32. A.V. Verkhovtsev, A.V. Korol, A.V. Solov'yov, J. Phys.: Conf. Ser. **490**, 012159 (2014)
33. U. Kreibig, M. Vollmer, *Optical Properties of Metal Clusters* (Springer-Verlag, Berlin, Heidelberg, 1995)
34. J.-P. Connerade, A.V. Solov'yov, Phys. Rev. A **66**, 013207 (2002)
35. A.V. Solov'yov, Int. J. Mod. Phys. B **19**, 4143 (2005)
36. A.V. Verkhovtsev, A.V. Korol, A.V. Solov'yov, Eur. Phys. J. D **66**, 253 (2012)
37. J. Lindhard, K. Dan. Vidensk. Selsk. Mat-fys. Medd. **28**, 8 (1954)
38. S. Agostinelli et al., Nucl. Instrum. Meth. A **506**, 250 (2003)
39. J. Allison et al., IEEE Trans. Nucl. Sci. **53**, 270 (2006)
40. L.G. Gerchikov, A.N. Ipatov, A.V. Solov'yov, J. Phys. B **30**, 5939 (1997)
41. L.G. Gerchikov, A.N. Ipatov, R.G. Polozkov, A.V. Solov'yov, Phys. Rev. A **62**, 043201 (2000)
42. L.G. Gerchikov, A.V. Solov'yov, J.-P. Connerade, W. Greiner, J. Phys. B **30**, 4133 (1997)
43. P. Bolognesi, A. Ruocco, L. Avaldi, A.V. Verkhovtsev, A.V. Korol, A.V. Solov'yov, Eur. Phys. J. D **66**, 254 (2012)
44. D. Östling, P. Apell, A. Rosen, Europhys. Lett. **21**, 539 (1993)
45. S. Lo, A.V. Korol, A.V. Solov'yov, J. Phys. B **40**, 3973 (2007)
46. A.V. Korol, A.V. Solov'yov, Phys. Rev. Lett. **98**, 179601 (2007)
47. S.W.J. Scully et al., Phys. Rev. Lett. **94**, 065503 (2005)
48. E. Scifoni, E. Surdutovich, A.V. Solov'yov, Phys. Rev. E **81**, 021903 (2010)
49. P. de Vera, R. Garcia-Molina, I. Abril, A.V. Solov'yov, Phys. Rev. Lett. **110**, 148104 (2013)
50. P. de Vera, R. Garcia-Molina, I. Abril, Phys. Rev. Lett. **114**, 018101 (2015)
51. P. de Vera, E. Surdutovich, I. Abril, R. Garcia-Molina, A.V. Solov'yov, Eur. Phys. J. D **68**, 96 (2014)
52. Geant4 Collaboration, *Physics Reference Manual*, viewed 11 June 2013, http://geant4.web.cern.ch/geant4/UserDocumentation/UsersGuides/PhysicsReferenceManual/BackupVersions/V9.6/fo/PhysicsReferenceManual.pdf
53. S. Guatelli, A. Mantero, B. Mascialino, P. Nieminen, M.G. Pia, IEEE Trans. Nucl. Sci. **54**, 585 (2007)
54. S. Chauvie et al., in *Proceedings of IEEE-NSS* (Rome, Italy, 2004)
55. S. Incerti et al., Med. Phys. **37**, 4692 (2010)
56. R. Kuzuo, M. Terauchi, M. Tanaba, Y. Saito, H. Shinohara, Jpn J. Appl. Phys. **30**, L1817 (1991)
57. H. Deutsch, K. Becker, J. Pittner, V. Bonacic-Koutecky, S. Matt, T.D. Märk, J. Phys. B **29**, 5175 (1996)
58. M.E. Rudd, Y.-K. Kim, D.H. Madison, T.J. Gay, Rev. Mod. Phys. **64**, 441 (1992)
59. M.E. Rudd, Y.-K. Kim, T. Märk, J. Schou, N. Stolterfoht, L.H. Toburen, *Secondary Electron Spectra from Charged Particle Interactions* (International Commission on Radiation Units and Measurements, Bethesda, MD, 1996) (ICRU 55)
60. E. Surdutovich, O.I. Obolensky, E. Scifoni, I. Pshenichnov, I. Mishustin, A.V. Solov'yov, W. Greiner, Eur. Phys. J. D **51**, 63 (2007)